Stalactite Growth as a Free-Boundary Problem: A Geometric Law and Its Platonic Ideal

Martin B. Short,[1] James C. Baygents,[2,3] J. Warren Beck,[1,4] David A. Stone,[5]
Rickard S. Toomey III,[6] and Raymond E. Goldstein[1,3]

[1]*Department of Physics, University of Arizona, Tucson, Arizona 85721, USA*
[2]*Department of Chemical and Environmental Engineering, University of Arizona, Tucson, Arizona 85721, USA*
[3]*Program in Applied Mathematics, University of Arizona, Tucson, Arizona 85721, USA*
[4]*Accelerator Mass Spectrometry Facility, University of Arizona, Tucson, Arizona 85721, USA*
[5]*Department of Soil, Water, and Environmental Science, University of Arizona, Tucson, Arizona 85721, USA*
[6]*Kartchner Caverns State Park, P.O. Box 1849, Benson, Arizona 85602, USA*

The chemical mechanisms underlying the growth of cave formations such as stalactites are well known, yet no theory has yet been proposed which successfully accounts for the dynamic evolution of their shapes. Here we consider the interplay of thin-film fluid dynamics, calcium carbonate chemistry, and CO_2 transport in the cave to show that stalactites evolve according to a novel local geometric growth law which exhibits extreme amplification at the tip as a consequence of the locally-varying fluid layer thickness. Studies of this model show that a broad class of initial conditions is attracted to an ideal shape which is strikingly close to a statistical average of natural stalactites.

The astonishing variety and beauty of structures found in limestone caves, from stalactites and stalagmites to soda straws, draperies, and helictites, have been the subject of human wonder for hundreds if not thousands of years [1]. There is little debate about the fundamental chemical processes responsible for their development. Water enters the cave from the overlying environment with significant concentrations of dissolved carbon dioxide and calcium. As the partial pressure of CO_2 in the cave is lower than that in the overlying rock, CO_2 outgases from the water. This raises the pH and leads to supersaturation and then precipitation of calcium carbonate. Yet, this chemical picture is only part of the story, for it does not in any direct way answer the most obvious morphological question: why are stalactites long and slender, often roughly conical? While some studies address the dynamics of speleothem morphology, [2–4], none quantitatively explains this most basic fact.

Here, we view the growth of stalactites as a free-boundary problem akin to those found in the theory of crystal growth [5], and derive a geometric law of motion in which the growth rate depends on the local radius and inclination of the stalactite surface. This approach is used to explain quantitatively the long, slender forms of stalactites by leading to the discovery of a universal shape toward which general initial conditions evolve. Found under a set of limiting assumptions, this may be thought of as the *Platonic ideal* of speleothem growth. While real stalactites have more complex shapes due to instabilities and cave inhomogeneities, we find that comparison with the average shapes of natural stalactites shows very good agreement. This work serves to emphasize a broad class of problems that demands considerable attention—*free-boundary dynamics in precipitative pattern formation*. Beyond speleothems, these include structures as diverse as hydrothermal

vents [6], chemical gardens [7], mollusc shells [8], and tubes whose growth is templated by bubbles [9]. Further development of greatly-accelerated model systems [10] to allow quantitative tests of such theories is thus an important goal.

The fluid layer flowing down the surface of a growing stalactite controls precipitative growth, so we first establish its typical thickness and velocity. Consider a cylindrical stalactite of radius R, length ℓ, over the surface of which flows an aqueous film of thickness h. We show below that the Reynolds number is low enough that the Stokes approximation is valid, and that $h \ll R$ over nearly the entire stalactite, so the velocity profile in the layer may be deduced by assuming a flat surface. Let y be a coordinate perpendicular to the surface and θ the tangent angle with respect to the horizontal [Fig. 1(a)]. The Stokes equation for gravity-driven flow is $\nu d^2u/dy^2 = g\sin\theta$, where $\nu = 0.01$ cm^2/s is the kinematic viscosity of water. No-slip and stress-free boundary conditions at the solid-liquid and liquid-air interfaces yield $u(y) = u_0[2(y/h) - (y/h)^2]$, where $u_0 = (gh^2/2\nu)\sin\theta$. The volumetric flux $Q = 2\pi R \times \int_0^h dy\, u(y) = (2\pi g/3\nu)Rh^3\sin\theta$. Measuring Q in cm^3/h
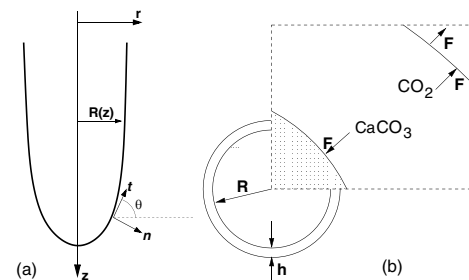

FIG. 1. Geometry of fluid flow along the surface of a stalactite (a) and model for determination of growth rate (b).
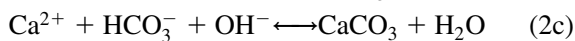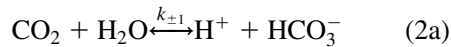
and R in cm, we find

$$h \simeq 11 \ \mu m \left(\frac{Q}{R \sin\theta}\right)^{1/3}, \qquad (1a)$$

$$u_0 \simeq 0.060 \ cm/s \left(\frac{Q^2 \sin\theta}{R^2}\right)^{1/3}. \qquad (1b)$$

Typically, $1 < R < 10$ cm and the flow rates are well below 100 cm^3/hr [11], so the layer thickness is tens of microns and the surface velocities below several mm/s. On the scale of the water layer thickness, the Reynolds number is $Re_w = u_0 h/\nu \sim 0.007(Q/R)$, well in the laminar regime, as anticipated. Of course, the thickness law (1a) will cease to hold near the bottom tip of the surface, where $\theta \sim 0$ and h would appear to diverge. In reality a pendant drop periodically detaches there, on a scale set by the competition between surface tension σ and gravity—the capillary length $l_c = (\sigma/\rho g)^{1/2} \sim 0.3$ cm. We see below that our theory dictates a small-distance cutoff that is subsumed within the capillary length.

Next we address gross features of the precipitation process. The accretion rate of calcium carbonate can be deduced from stalactite elongation rates v, which are ~ 1 cm/century. Since stalactites are so slender, the volumetric increase can be estimated by considering the addition of a disk at the top of the stalactite, where the typical radius is ~ 5 cm. Hence, ~ 80 cm^3 or ~ 200 g of CaCO$_3$ is added per century. Assuming a volumetric flow rate of ~ 40 cm^3/h, toward the lower end of the measured range [11], the volume of water that flows over the stalactite in a century is $\sim 36\,000$ liters. With a typical concentration of calcium in solution of 150 ppm (mg/l), the total mass of calcium in that fluid volume is 5.4 kg, yielding a fractional precipitation of ~ 0.04, sensibly small given the ubiquity of stalagmites below stalactites [12].

The dependence of the precipitation rate on fluid layer thickness is crucial; we extend important earlier work [13] to derive this. Consider a growing spherical body covered by fluid and surrounded by still atmosphere in which CO$_2$ diffuses [Fig. 1(b)]. The fluid has average calcium ion concentration $\overline{[Ca^{2+}]}$ and proton concentration $[H^+]$, the latter assumed constant in the layer, as is valid for thin films. The ratio $\epsilon \equiv h/R$ is an important small parameter. Of the chemical reactions occurring in the fluid layer, the most important are [13]:

$$CO_2 + H_2O \underset{k_{\pm 1}}{\longleftrightarrow} H^+ + HCO_3^- \qquad (2a)$$

$$CO_2 + OH^- \underset{k_{\pm 2}}{\longleftrightarrow} HCO_3^- \qquad (2b)$$

$$Ca^{2+} + HCO_3^- + OH^- \longleftrightarrow CaCO_3 + H_2O \qquad (2c)$$

$$H^+ + CO_3^{2-} \longleftrightarrow HCO_3^-. \qquad (2d)$$

It is critical to note that for each molecule of CaCO$_3$ that adds to the surface of the crystal, one molecule of CO$_2$ must be generated in the solution via pathways (2a) and (2b), whose relative importance depends upon pH. Hence, for growth (or dissolution) to occur, CO$_2$ and HCO$_3^-$ must

not be in chemical equilibrium. Of course, (2c) lies outside of equilibrium as well, but can be shown to be fast compared to (2a) and (2b) in the case of thin films, so that it is not rate-limiting. Reaction (2d), on the other hand, will be considered always equilibrated, leaving $[HCO_3^-]$, $[CO_3^{2-}]$, and $[H^+]$ related by the equilibrium constant K. Therefore, through the use of an electroneutrality condition, $[HCO_3^-]$ may be expressed solely in terms of $[H^+]$ and $[Ca^{2+}]$ as

$$[HCO_3^-] = \frac{2[Ca^{2+}] + (1-\beta)[H^+]}{1 + 2\alpha}, \qquad (3)$$

where $\alpha = K/[H^+]$, $\beta = K_W/[H^+]^2$, and K_W is the water dissociation constant.

To derive a growth law, we find the flux of Ca^{2+} onto the surface of the sphere from the diffusion equation

$$\partial_t[Ca^{2+}] = D_{Ca^{2+}} \nabla^2[Ca^{2+}]. \qquad (4)$$

We impose upon $[Ca^{2+}]$ zero flux at $r = R + h$ and a flux $-F$ at $r = R$ for all t, and employ our knowledge of $\overline{[Ca^{2+}]}$ at $t = 0$. All diffusive transients are assumed to have decayed, so $\partial_t[Ca^{2+}]$ is a constant. The dynamics of $[CO_2]$ are assumed to be in quasi-steady state; therefore, substituting (3) into the chemical dynamics of the reaction-diffusion equation for CO$_2$ leaves us with

$$D_{CO_2}\nabla^2[CO_2] = k_+[CO_2] - k_-[Ca^{2+}] - k_0, \qquad (5)$$

where

$$k_0 \equiv \frac{1}{2}(1 - \beta)k_-[H^+], \qquad (6a)$$

$$k_+ \equiv k_{+1} + \beta k_{+2}[H^+], \qquad (6b)$$

$$k_- \equiv \frac{2(k_{-1}[H^+] + k_{-2})}{1 + 2\alpha}. \qquad (6c)$$

We impose zero flux of $[CO_2]$ at $r = R$ and flux $F/(1 + \epsilon)^2$ at $r = R + h$, recalling that the number of Ca^{2+} molecules deposited equals the number of CO$_2$ molecules released. Finally, since diffusion of atmospheric carbon dioxide $[CO_2]_a$ is in steady state, we have the Stefan condition

$$\nabla^2[CO_2]_a = 0, \qquad (7)$$

with boundary conditions of a flux $F/(1 + \epsilon)^2$ at $r = R + h$ and an asymptotic value of $[CO_2]_\infty$.

To find the growth rate, we must solve the simultaneous diffusion equations that hold in each domain, subject to boundary conditions. The lengthy details of this calculation will be presented elsewhere. Here, we summarize them as follows: solve (4) in terms of F and $\overline{[Ca^{2+}]}$, use this solution at $t = 0$ in (5) to find $[CO_2]$ in terms of these same quantities, solve (7) in terms of F and $[CO_2]_\infty$, use the solutions to (5) and (7) to find $[CO_2]$ and $[CO_2]_a$ at $r = R + h$, relate the two through Henry's constant H, and thus deduce F. For a sphere, one finds

$$F \simeq h(k_-\overline{[Ca^{2+}]} + k_0 - k_+ H[CO_2]_\infty)$$

$$\times \left[1 + \epsilon\left(1 - \frac{HR^2 k_+}{D_a}\right) + O(\epsilon^2)\right]. \qquad (8)$$

Note that F does not depend explicitly upon atmospheric diffusion until order ϵ. This first correction takes the form of a ratio of the time scale for diffusion of the newly created CO_2 into the atmosphere to that for conversion of CO_2 back into HCO_3^-. It is also very small, being only $\sim 10^{-3}$. In contrast with other dendritic growth phenomena [5], atmospheric diffusion is not rate-limiting, and thus the dynamics is local.

If the local concentration gradients within the fluid are dominantly perpendicular to the flow within the layer, then advective contributions to precipitation can be ignored in computing the growth rates. In the present calculation, where we ignore instabilities that can produce ripples, where the *diffusion time* $t_D = h^2/D \sim 0.1$ s for equilibration in the layer is extremely small compared to the *contact time* $t_\ell = \ell/u_0 \sim 10^3$ s for a fluid parcel to traverse the typical length $\ell \sim 100$ cm of the stalactite, and where t_ℓ itself is extremely small compared to the *growth time* $t_v = h/v \sim 10^7$ s; this is a valid approximation. Hence, it follows from (1a) and (8) at leading order that there is a *geometrical* law for growth in which the component of the growth velocity **v** normal to the surface is given by the local radius $r(z)$ and tangent angle θ,

$$\hat{\mathbf{n}} \cdot \mathbf{v} = v_c \left(\frac{\ell_Q}{r \sin\theta} \right)^{1/3}, \tag{9}$$

where $v_c = v_m \ell_Q (k_- \overline{[Ca^{2+}]} + k_0 - k_+ H[CO_2]_\infty)$ is the characteristic velocity, v_m is the molar volume of $CaCO_3$, and $\ell_Q = (3\nu Q/2\pi g)^{1/4} \sim 0.01$ cm is a characteristic length. The velocity v_c depends upon the pH through k_0 and $k_\pm$, crossing from positive (growth) to negative (dissolution) at a critical pH that depends on $\overline{[Ca^{2+}]}$ [Fig. 2(a)]. Cave water is close to the typical crossing point, giving $v_c \sim 0.1$ mm/yr, quite consistent with observations.

The growth model (9) generalizes the work of Kaufmann [4] by explicit inclusion of the dependence of film thickness on stalactite radius and surface inclination—that is, it recasts the dynamics as a true free-boundary problem. As a model for axisymmetric surface evolution, Eq. (9) depends on the absolute orientation of the surface through θ, as it must when gravity breaks the symmetry and drives the fluid flow. As such, it differs fundamentally from geometrical models of interface evolution [14], which depend only on invariants such as the curvature $\kappa = \partial\theta/\partial s$. Its dependence on angle is reminiscent of the effects of surface tension anisotropy [5], but with a vastly more singular form [Fig. 2(b)] producing a high and rapidly-varying growth rate near the tip, where θ is small, and a roughly constant growth rate for the nearly vertical regions ($\theta \sim \pi/2$). This extreme amplification near the tip produces the slender form of stalactites.

Numerical studies of this growth law [Fig. 2(c)] show that an initially rounded shape develops a conical instability at its lowest point; a downward bump, which has a smaller local radius, also has a locally thicker fluid layer in order
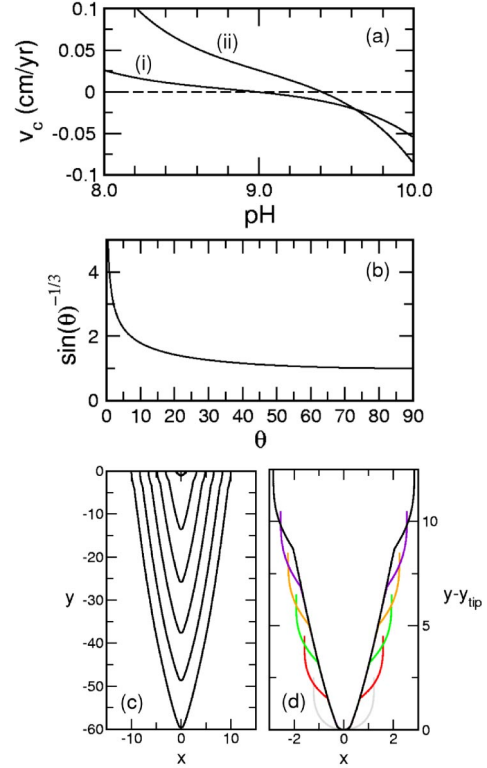

FIG. 2 (color online). Aspects of the growth law. (a) Growth velocity v_c versus pH, using CO_2 partial pressure in the cave atmosphere of 3×10^{-4} atm, a temperature of 20 °C, (i) $\overline{[Ca^{2+}]}$ of 100 ppm and volumetric fluid flow $Q = 2$ cm^3/h, and (ii) $\overline{[Ca^{2+}]} = 300$ ppm and $Q = 20$ cm^3/h. Formulas for constants taken from [13]. (b) The function of tangent angle θ in Eq. (9). (c) A rounded initial condition evolves into a fingered shape. (d) Aligning the tips of the growing shapes in (c) shows at early times a rapid collapse to a common form.

to conserve mass. This increased thickness produces a higher precipitation rate and the protuberance grows. Interestingly, the growing tip approaches a uniformly translating shape for a wide range of initial conditions [Fig. 2(d)]. This asymptotic shape $z(r)$ can be found by noting that the normal velocity (9) at any point on such a surface must equal $v_t \cos\theta$, where v_t is the tip velocity. Observing that $\tan\theta = dz/dr$ and rescaling symmetrically r and z as $\rho \equiv (r/\ell_Q)(v_t/v_c)^3$ and $\zeta \equiv (z/\ell_Q)(v_t/v_c)^3$ yields the differential equation

$$\frac{\zeta'(\rho)}{[1 + \zeta'(\rho)^2]^2} - \frac{1}{\rho} = 0. \tag{10}$$

Equation (10) has no real solution at $\rho = 0$. This is to be expected as the growth law (9) can not be valid exactly at the tip, where capillarity must modify the thickness of the film. The first real solution appears at $\rho = \rho_m \equiv 16/3\sqrt{3}$, and for $\rho > \rho_m$, there are two distinct real solutions of (10) for ζ', the solution of interest having $\zeta'' \geq 0$. Since $\ell_Q \sim 0.01$ cm, and assuming that $v_t \gtrsim v_c$, r_m will be much less than the capillary length, so this solution is valid every-
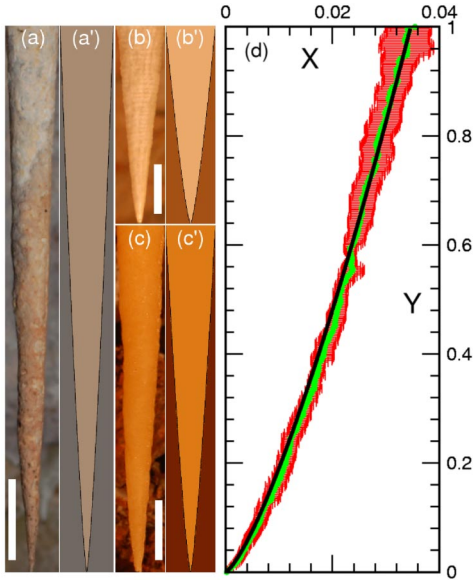
FIG. 3 (color online). Comparison between observed stalactite shapes and the Platonic ideal. Three examples (a)–(c) are shown, each next to an ideal shape of the appropriate aspect ratio and size (a')–(c'). Scale bars in each are 10 cm. (d) Master plot of stalactite shapes, rescaled as described in text. The average of 20 stalactites is shown with green circles and red uncertainties, and compared with the ideal (black curve).

where except the stalactite tip. One easily verifies that at large ρ there is a power-law form $\zeta \sim \rho^{4/3}$, which, while close to the conical form $\zeta \sim \rho$, produces an aspect ratio $\delta = \ell/w$, with ℓ the length and w the width, that increases with overall length. A systematic expansion yields the quite accurate approximation

$$\zeta(\rho) \simeq \frac{3}{4}\rho^{4/3} - \rho^{2/3} - \frac{1}{3}\ln\rho + \text{const.} \qquad (11)$$

A direct test of the relevance of the Platonic ideal was achieved by comparing it to the shapes of natural stalactites. Using a high-resolution digital camera, images of many stalactites in Kartchner Caverns (Benson, AZ) were recorded, each with a pair of fiducial marks projected from two parallel lasers to provide a local scale. It is important to emphasize that because the rescalings used to derive Eq. (10) are symmetric in r and z, a direct comparison between actual stalactites and the ideal requires only a global rescaling of the image. Moreover, as δ for the ideal increases with ℓ, this theory predicts that all stalactites will lie on the ideal curve provided the differential equation defining that curve is integrated up to a suitable length. Therefore, we can visually compare stalactite images to the ideal shape rather simply; Fig. 3 shows three representative examples of such a direct comparison, and the agreement is very good. Deviations are of course noted at the tip, where capillarity effects associated with the pendant drops alter the shape. For a more precise comparison, we extracted the contours of 20 stalactites by a standard edge-detection algorithm applied to the

images, yielding $r(z)$ for each. The optimal scaling factors for each were found by a least squares comparison with the ideal function. Finally, this set of rescaled data was averaged and compared directly to the theoretical curve [Fig. 3(d)]. Since each of the stalactites has a different length, fewer images contribute to the average the further from the tip one looks, hence the larger error bars further up the stalactite. The agreement between the data and theory is excellent; the Platonic form lies uniformly within 1 standard deviation of the mean.

The dynamic and geometric results presented here illustrate that the essential physics underlying stalactite shape is the locally-varying fluid layer thickness controlling the precipitation rate. Such physics is the basis for a stability analysis that may explain ripples often found on speleothems, similar to those on icicles [15]. Indeed, since icicle formation involves both thin-film fluid flow and diffusion (of latent heat), it is likely that an analysis like that here may explain the characteristic slender shapes of icicles as well. More generally, by highlighting the interplay between surface geometry and growth this work provides a starting point for a comprehensive explanation of the richness of speleothem morphology.

[1] C. Hill and P. Forti, *Cave Minerals of the World* (National Speleological Society, Inc., Huntsville, AL, 1997).
[2] H. W. Franke, Studies in Speleology **1**, 89 (1965).
[3] W. Dreybrodt, Boreas **28**, 347 (1999).
[4] G. Kaufmann, Earth Planet. Sci. Lett. **214**, 251 (2003).
[5] D. A. Kessler, J. Koplik, and H. Levine, Adv. Phys. **37**, 255 (1988).
[6] J. B. Corliss *et al.*, Science **203**, 1073 (1979).
[7] S. Thouvenel-Romans, W. van Saarloos, and O. Steinbock, Europhys. Lett. **67**, 42 (2004).
[8] E. Bonucci, *Calcification in Biological Systems* (CRC Press, Boca Raton, FL, 1992).
[9] D. A. Stone and R. E. Goldstein, Proc. Natl. Acad. Sci. U.S.A. **101**, 11537 (2004).
[10] L. C. Huff, J. Geol. **48**, 641 (1940).
[11] *Final Report: Environmental and Geologic Studies for Kartchner Caverns State Park*, edited by R. H. Beucher (Arizona Conservation Projects, Inc., Tucson, AZ, 1992).
[12] Depletion is negligible only when the rate-limiting step is not surface growth. At high Q and low $[Ca^{2+}]$, formation of $CaCO_3$ is rate-limiting and Ca^{2+} depletion, not CO_2 creation, controls the shape.
[13] D. Buhmann and W. Dreybrodt, Chemical Geology **48**, 189 (1984).
[14] R. C. Brower, D. A. Kessler, J. Koplik, and H. Levine, Phys. Rev. A **29**, 1335 (1984).
[15] K. Ueno, Phys. Rev. E **69**, 051604 (2004).